Extended interactions in the phase of oxygen

S. F. Agnew, B. I. Swanson, and L. H. Jones

Citation: J. Chem. Phys. **86**, 5239 (1987); doi: 10.1063/1.452547
View online: http://dx.doi.org/10.1063/1.452547
View Table of Contents: http://jcp.aip.org/resource/1/JCPSA6/v86/i10
Published by the American Institute of Physics.

Extended interactions in the ϵ phase of oxygen

S. F. Agnew, B. I. Swanson, and L. H. Jones
Los Alamos National Laboratory, University of California, Los Alamos, New Mexico 87545

(Received 2 February 1987; accepted 12 February 1987)

The high pressure infrared and Raman spectra for the ϵ phase of a series of oxygen samples, $^{16}O_2$, $^{16}O_2$ with 10% $^{18}O_2$, and $^{18}O_2$ with 6% ^{16}O ^{18}O, are reported. Assignments are made for the fundamental, combination, and isotope-induced features of this phase of solid oxygen based on a simple model that incorporates a pairwise interaction betweeen nearest-neighbor oxygen molecules within the molecular oxygen plane, with pairs forming extended chains. Vibrational analysis on this chain with two interaction force constants reproduces all of the features that we have observed.

INTRODUCTION

Two features common to nearly all of oxygen's solid phases are the rigorous parallel alignment of all the O–O intramolecular bonds and the existence of O_2 molecular planes normal to that same O–O bond axis, both features of which stand in sharp contrast to those of the structures of all of the other homonuclear diatomic solids.[1] In particular, in spite of the fact that fluorine is very similar to oxygen in size, both of its solid phases possess tilted molecules. Oxygen is somewhat unique, then, in that its intermolecular interactions result in the strict collinearity of the oxygen molecules in nearly every solid phase. It has been suggested[2] that the tendency of oxygen to remain strictly collinear and coplanar in all of its other phases is related to a spin–spin interaction, and this may very well contribute significantly to the stabilization energy of solid oxygen. However English and Venables have concluded[1] that the β-O_2 ($R\ \bar{3}m$) structure is stable due to oxygen's small quadrupole moment as well as its small d/σ (the elongation parameter in the Lennard-Jones potential). The further inclusion of an exchange energy interaction term in the potential energy function stabilizes[3] the α-O_2 lattice, which is the lowest temperature form of solid oxygen at zero pressure. As pressure increases, the δ phase of oxygen, which only exists at high pressure and is related[4] to α-O_2 by an interplanar shear, becomes stable. The δ-O_2 evidently retains the antiferromagnetic ordering of the α phase even at substantial pressure.

Above 10.0 GPa at room temperature, the ϵ phase of oxygen occurs. Although this high pressure of oxygen has received a great deal of attention by a number of investigators,[4–7] its structure and even the nature of its dark red color have not as yet been adequately explained, although it has been suggested[5] that the visible absorption spectrum of the dark red ϵ-O_2 is due to a closing of the gap between the isolated molecule states with $\pi^4\pi^{*2}$ and $\pi^3\pi^{*3}$ configurations. Our previous work has reported[6] on the strong infrared absorption for this phase of oxygen as well as an unexpected doubling of the Raman band for a sample of $^{18}O_2$ with 6% ^{16}O ^{18}O. We concluded[6] that the onset of the ϵ phase was associated with strong intermolecular interactions, that the ϵ-O_2 structure is centric, and that the primitive unit for this lattice was at least two molecules and possibly four. The behavior of the infrared and Raman features as a function of pressure further indicated that the O–O molecular bond was weakening at the expense of an increasing intermolecular interaction. This further work seeks to complete and extend our previous work and report the spectral characteristics over a much wider range of pressures and samples than we reported previously. In addition, we have developed a structural model that is consistent with the data obtained over a wide pressure range and isotopic composition.

A recent report on the powder pattern x-ray diffraction of ϵ-O_2 has concluded[7] that an orthorhombic distortion of the δ phase comes close to explaining the diffraction data. These authors further argued that an 8%–10% volume decrease occurs upon entering the ϵ phase and since the interplanar diffraction line at 3.40 Å does not change discontinuously upon entering the ϵ phase, this contraction must take place within the molecular oxygen planes. Although not stated by the authors, the appearance of a diffraction line at 4.48 Å in the ϵ phase proves that the primitive unit cell has doubled, and considering the intraplanar volume decrease, it is reasonable to conclude that this doubling has occurred along one of the two axes of the molecular oxygen plane.

One of the interesting properties of ϵ-O_2 is its strong infrared absorption at the O=O stretch fundamental. Early reports[8,9] of an infrared absorption in thin layers of solid oxygen at low temperature and zero pressure and a more recent report[10] indicate that a new metastable crystalline phase of oxygen, m-O_2, forms with vapor deposition onto a surface that is in the temperature 8–11 K. The m-O_2 infrared absorption spectrum showed evidence for four distinct molecular oxygen sites and isotopic mixtures indicated an eight molecule unit cell. We do not believe, then, that m-O_2 has anything more in common with the ϵ phase than the fact that it also absorbs infrared. Thus, we find that the high density of the ϵ phase is simply a contributing factor to the appearance of an infrared absorption in ϵ-O_2, and that any of the oxygen phases would undergo infrared absorption were it not for the fact that only one molecule of oxygen occupies each primitive unit for most of oxygen's phases, although the intensity of that absorption will be dependent on the strength of the intermolecular coupling.

EXPERIMENTAL

Diamond anvil cells designed[11] after Merrill and Bassett with either type Ia or IIa diamonds were used to study oxygen in the pressure range 5–20 GPa at room temperature. Sepa-

 0021-9606/87/105239-07$02.10

rate samples of isotopically pure $^{16}O_2$, $^{18}O_2$ containing 6% ^{16}O ^{18}O, and $^{16}O_2$ containing 10% $^{18}O_2$ were loaded[12] using the indium-dam technique. Pressures were measured[13] by the ruby fluorescence method, assuming the R_1 line shift to be 0.1328 GPa/cm^{-1}. Infrared spectra were obtained with a Digilab FTS-20CV equipped with a Hg–Cd–Te detector and appropriate home-built beam condensor. Typically, 100 scans at 2 cm^{-1} resolution were signal averaged to produce a spectrum.

Raman spectra were obtained in a backscattering geometry by using various lines from Spectra Physics model 171 argon and krypton ion lasers. The Raman scattered light was collected with a SPEX model 1403 double monochromator equipped with a Nicolet data station. Typically, resolution was 3 cm^{-1} for the spectra collected.

The fundamental vibrations of the structural model were calculated by means of the FG harmonic approximation where the O_2 vibrations are coupled by means of off-diagonal matrix elements of F, the force constant matrix, and isotopic composition is treated by adjusting the terms of the G matrix. Since the libron frequency[6] is 130 cm^{-1} the diagonal force constant between neighboring molecules is expected to be small and is neglected. The three parameters, the diagonal force constant for the O–O stretch f_1, the nearest-neighbor interaction force constant f_2, and the next-nearest-neighbor interaction force constant f_3, were adjusted to give a resonable fit to the observed infrared and Raman frequencies for $^{16}O_2$ at 12.0 GPa. We note that the low frequency infrared combination was used to determine f_3, which represents coupling between primitive units (see the Discussion). This model incorporates a linear chain of molecular oxygen pairs, each molecule having an identical diagonal force constant f_1, an off-diagonal interaction force constant f_2 for the three nearest neighbors, both along the chain axis as well as between the oxygens of each pair, and an off-diagonal interaction force constant f_3 between next-nearest neighbors along the chain axis, where we have ignored interchain interactions (see Fig. 1). This particular model was chosen so as to be consistent with a variety of observations about ϵ oxygen as well as to allow a fairly simple description of the undetermined lattice. In the harmonic approximation, the solution to the vibrational eigenvalue problem is equivalent to diagonalizing the so-called FG matrix. The F matrix contains force constants for the various motions of the system while the G matrix contains information about the reduced masses of those same motions. Thus, F represents the potential energy part of the harmonic oscillator Hamiltonian and G holds the mass and kinetic energy information. Since our G matrix is diagonal, solution of the eigenvalue problem reduces to diagonalization of the Hermitian eigenvalue matrix $\mathbf{G}^{1/2}\mathbf{F}\mathbf{G}^{1/2}$, providing the eigenvalues and eigenvectors that are the frequencies and amplitudes for the corresponding normal modes of the problem.

RESULTS

The observations of strong infrared absorptions (fundamental and combination) in ϵ-O_2 and the appearance of a $^{16}O^{18}O$ impurity-induced doubling of the Raman band in $^{18}O_2$, have been reported[6] in a previous letter and we now report the pressure dependences of these same features. Figures 2 and 3 show frequencies of these various features plotted as a function of pressure at room temperature. The infrared features appear abruptly at around 10 GPa, shift to lower frequency until about 14 GPa, and then do not change significantly as a function of pressure up to the limits of our measurements ($\sim$20 GPa). We note that our previous work erroneously reported[6] a splitting in the infrared fundamental for pressures above 15.0 GPa. During this same pressure interval, the bulk Raman peak shifts up following an initial

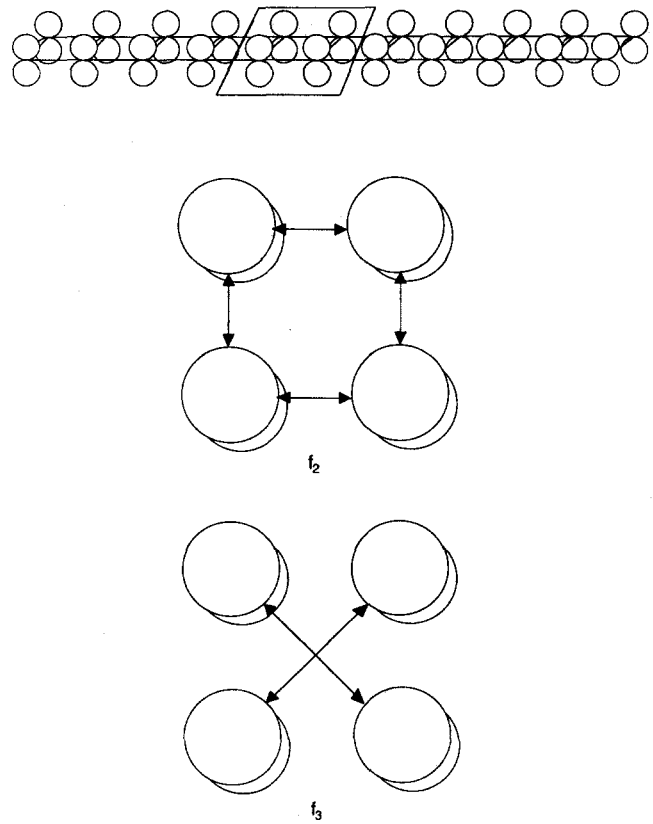

FIG. 1. Description of the model showing interaction force constants that are used. View is down O–O bond axis.

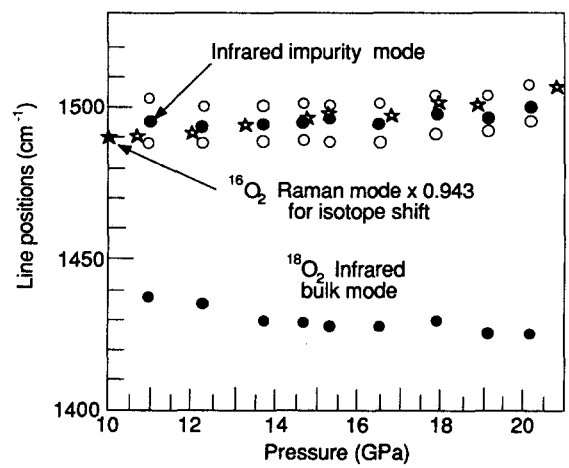

FIG. 2. Pressure dependence of Raman (○) and infrared (●) features for 6% ^{16}O ^{18}O in $^{18}O_2$. Also shown is the pressure dependence of the single Raman band (*) for $^{16}O_2$ scaled by 0.943, the expected shift due to the change in mass.

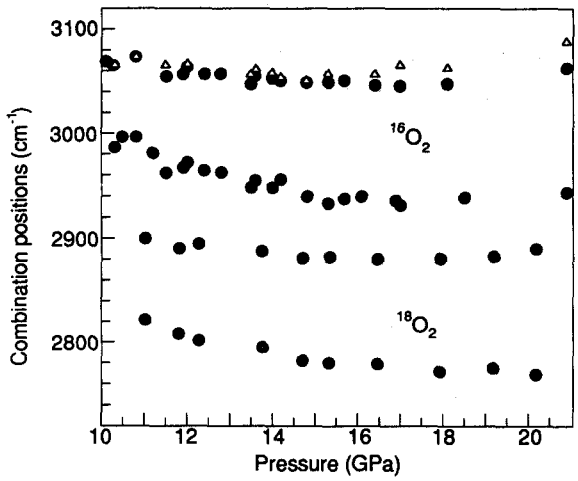

FIG. 3. Pressure dependences of infrared combinations for $^{18}O_2$ (lower) and $^{16}O_2$ (upper) as well as calculated value (Δ) of upper combination for $^{16}O_2$ based on $\nu_{\text{infrared}} + \nu_{\text{Raman}} - 25\ \text{cm}^{-1}$.

drop in frequency after crossing the ϵ-O_2 phase boundary at 10 GPa. The combination bands (Fig. 3) shift to lower frequency with increasing pressure, following the trend of the infrared fundamental. The rates at which the two combinations change with increasing pressure differ, and this fact aids in their assignments. We assign the high frequency feature to a combination involving zone center Raman and infrared fundamentals resulting in an anharmonicity of 25 cm^{-1} (see Table I), which is completely consistent with the gas phase value of 24 cm^{-1} for free oxygen. The pressure dependence of this combination calculated from the fundamentals is indicated in Fig. 3 as well, illustrating the fact that this assignment is consistent with the behavior of the fundamentals and that the anharmonicity is not pressure dependent under 16.0 GPa, but does change slightly above this pressure.

The lower frequency combination band, on the other hand, is most likely due to a combination of zone boundary motions of the infrared and Raman fundamentals such that the sum of the wave vectors is zero, i.e., $k_{\text{Raman}} + k_{\text{infrared}} = 0$. Thus, the value of this combination represents the combined dispersion of the in- and out-of-phase motions at the zone boundary. An alternative explanation might involve the combination of two infrared fundamentals. We reject this, however, since not only are noncentric lattices very uncommon with homonuclear diatomic solids, but there is strict exclusion between the Raman and infrared features that we see as well. Yet another explanation supposes the existence of inactive zone center modes (i.e., a cell quadrupling). We also reject this due to the fact that we can find no factor group that produces an inactive infrared vibration following cell quadrupling. More precisely, the symmetry species produced by coupling four oxygen vibrations together are never both infrared and Raman inactive for any resonable model.

In support of the zone boundary nature of the low frequency combination is the fact that more structure appears around the two main combination features as pressure increases. We attribute this additional structure to the presence of dispersion along differing k-vector directions and therefore to a variation of the vibron density of states (i.e., spectral peaks correspond to points in the Broullion zone with high density of states).

The behavior of the Raman bands as a function of pressure is shown in Figs. 2 and 4 for a sample of 6% ^{16}O ^{18}O in $^{18}O_2$. At 8.7 GPa we observe bands at 1496 and 1518 cm^{-1} distinct from the bulk $^{18}O_2$ band, which appears at 1492 cm^{-1}. Note that the band at 1518 cm^{-1} has a shoulder at 1521 cm^{-1} that we cannot assign. These spectra are from β-O_2 and the two impurity features can be explained on the basis of a band due to $^{18}O_2$ perturbed by neighboring ^{16}O ^{18}O as well as one due to the ^{16}O ^{18}O itself, respectively. The isotope shift and relative intensity betweeen these two features do not agree with the expected values for the ^{16}O ^{18}O band, 1537 (calc.) vs 1518 (meas.) cm^{-1} and 6%(calc.) vs 16%(meas.), which indicates that there is a significant in-

TABLE I. Observed and calculated frequencies for ϵ-O_2.

Sample	Obs. Freq.[a]	Calc. Freq.[a]	Assignment
$^{16}O_2$	1512	1520	infrared $k=0$
at 12.0 GPa	1579	1579	Raman $k=0$
	2972	2972(20)	$R(k=\pi/a)+\text{IR}(k=-\pi/a)$ comb.
	3066(25)	3074(25)	$R(k=0)+\text{IR}(k=0)$ combination
6% ^{16}O ^{18}O in $^{18}O_2$	1437	1432	infrared $k=0$
at 12.3 GPa	1486	1487	Raman_1
	1495	1494	Infrared of pair site
	1502	1500	Raman_2
	2811	2811(11)	$R(k=\pi/2)+\text{IR}(k=-\pi/a)$ comb.
	2892(31)	2888(31)	$R(k=0)+\text{IR}(k=0)$combination
10% $^{18}O_2$ in $^{16}O_2$	1423	1430	Infrared of $^{18}O_2$ site
at 11.2 GPa	1446	1470	Infrared of ^{16}O ^{18}O site
	1515	1519	infrared $k=0$
	1575	1578	Raman $k=0$
	2981	2981(11)	$R(k=\pi/a)+\text{IR}(k=-\pi/a)$ comb.
	3055(35)	3062(35)	$R(k=0)+\text{IR}(k=0)$ combination

[a] Anharmonicities, where appropriate, in parentheses.

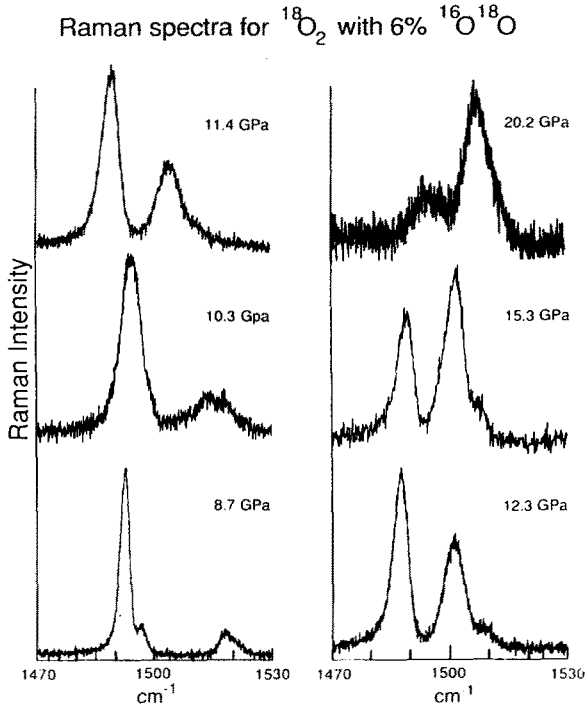

FIG. 4. Raman spectra at various pressures for 6% ^{16}O ^{18}O in $^{18}O_2$. The ϵ phase occurs at 10 GPa, but spectra only exhibit pure ϵ phase character above 11 GPa.

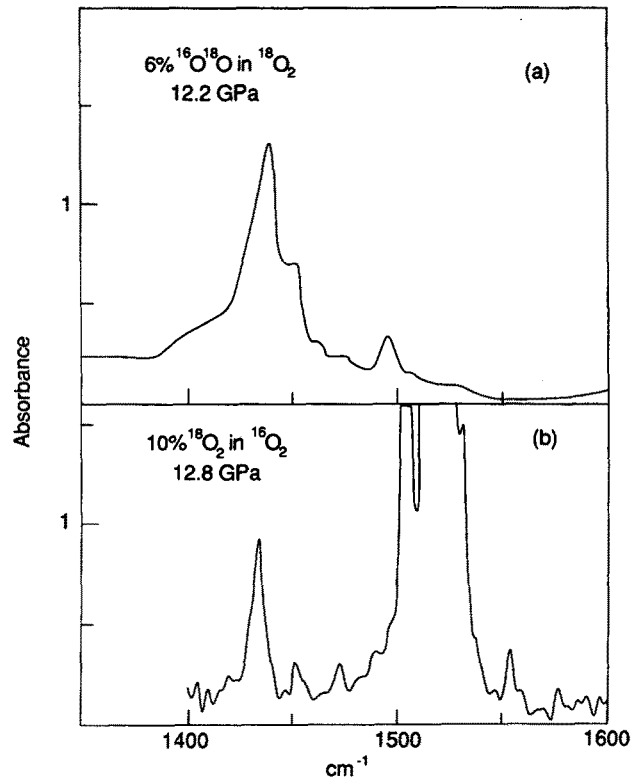

FIG. 5. Infrared spectra of (a) 6% ^{16}O ^{18}O in $^{18}O_2$ at 12.3 GPa and (b) 10% $^{18}O_2$ and 0.6% ^{16}O ^{18}O in $^{16}O_2$ at 12.8 GPa.

teraction between oxygen molecules even in the β phase. In contrast to these spectra for β-O_2, fluid oxygen below 5.5 GPa has both isotope shifts and relative intensities within 1% of the expected values. As pressure is increased to 11.4 GPa, these two impurity induced bands disappear and a single band at 1504 cm^{-1} with a shoulder at 1511 cm^{-1} results. In the intermediate pressure regime, it is very difficult to obtain single phase spectra because the ϵ phase undergoes laser heating due to its strong visible absorption and, since we are very close to the 10 GPa phase boundary, the spectrum reflects some steady-state mixture of the two phases. The spectrum at 10.3 GPa is an example of such a mixture. Once pressure is increased further, the "impurity" band increases in intensity until, at about 14 GPa, it becomes the dominant feature.

A mixed isotope sample of $^{16}O_2$ with 10% $^{18}O_2$ and 0.6% ^{16}O ^{18}O was prepared and loaded. Doubling of the Raman band was not observed, although we did observe impurity-induced infrared bands as well as significant broadening on the low frequency side of the bulk infrared absorption, suggesting that another band is present. A well defined impurity-induced infrared band appears at 1423 cm^{-1} at 11.2 GPa [see Fig. 5(b)], which is consistent with the expected isotope shift for $^{18}O_2$ based on $^{16}O_2$, that is, 0.943×1515 cm^{-1} = 1429 cm^{-1}. In sharp contrast to the isotopic shift anomolies that we observed for the 6% ^{16}O ^{18}O in $^{18}O_2$, then, for the 10% $^{18}O_2$ in $^{16}O_2$ sample, the $^{18}O_2$ infrared band position is not anomolous. A band at 1451 cm^{-1} [Fig. 5(b)] is evidently due to the 0.6% ^{16}O ^{18}O in the sample, although the isotope shift predicts $0.97 \times 1515 = 1470$ cm^{-1}. This anomolous isotope shift for an infrared band position, we expect, is related to the anomolous isotope shifts of the Raman bands for the 6% ^{16}O ^{18}O in $^{18}O_2$ sample. The doubling or increased width that appears on the low energy side of the bulk infrared absorption is evidently due to the 10% $^{18}O_2$ impurity. Comparison of this band with that observed in neat $^{16}O_2$ samples indicates that something is indeed increasing the absorption on the low energy side of this feature. Other less intense features that appear as pressure increases (i.e., 1470 and 1555 cm^{-1}) are evidently due to higher order sites, where adjacent impurities couple.

DISCUSSION

All of the known three-dimensional oxygen structures consist of parallel planes of colinear oxygen molecules except for γ-O_2, which exists over a relatively narrow pressure–temperature range. Two structural details that we know about the ϵ phase from previous work are[7]: (1) The powder diffraction line due to the planes of collinear oxygens does not change discontinuously across the ϵ phase boundary. This suggests very strongly that this particular plane, which is so ubiquitous in the phases of solid oxygen, is also present in ϵ-O_2. (2) Based upon the increased loading necessary to cross the ϵ phase boundary, as well as the volume of an approximate orthorhombic cell fit to the diffraction data, an estimated 8%–10% volume decrease occurs upon entering the ϵ phase. Details (1) coupled with (2) indicate that, while a great deal of structural change occurs within the oxygen molecular planes, no appreciable interplanar changes occur. In trying to reconcile the spectroscopic observations reported here, these constraints are very useful in defining a structural model.

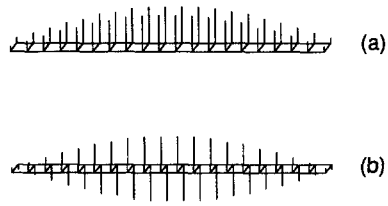

FIG. 6. Amplitudes (vertical lines) of the O–O stretches for the model lattice 42 molecules showing the zone center motions for the (a) Raman and (b) infrared modes. An oxygen molecule sits at every vertex.

We include only the O–O stretching motion and its nearest- and next-nearest-neighbor interactions, finding the energies and amplitudes for the in-phase and out-of-phase motions of the oxygen pair that constitutes the primitive unit. These motions correspond to the Raman- and infrared-active bulk modes of the solid, respectively. When we calibrate the model with the observed infrared and Raman fundamental and infrared combination frequencies from $^{16}O_2$, the resultant eigenvectors take on amplitudes as shown in Fig. 6(a) with $f_1 = 10.931$, $f_2 = 0.195$, and $f_3 = 0.120$ mdyn/Å. With the finite boundary conditions used in this model of 20 (or 21) pairs of oxygen molecules, the zone center symmetric and antisymmetric motions are well represented as shown in Fig. 6. We use a model that is sufficiently large so as to minimize edge effects when an impurity is inserted in the middle of the chain. When a single impurity with a smaller reduced mass (^{16}O ^{18}O in $^{18}O_2$) is placed in the model lattice, two Raman-active modes (i.e., totally symmetric modes) are generated [Figs. 7(a) and 7(b)] with the impurity either in phase or out of phase with the rest of the chain. This is in contrast to what occurs when an impurity with a larger reduced mass is placed in the model lattice (i.e., $^{18}O_2$ in $^{16}O_2$), where the impurity couples more strongly with the infrared active bulk mode [see Fig. 7(c)]. That is, in any coupled harmonic oscillator problem, an impurity oscillator with a different frequency will have more amplitude in either the symmetric or the antisymmetric bulk motion depending both on whether the impurity frequency is higher or lower than that the bulk and on the sign of the coupling constant between oscillators. In fact, a related problem has already been addressed[14] by Decius with regards to the out-of-plane bending mode in nitrates and carbonates of the linear chain aragonite structure. Decius was attempting to explain the anomolous integrated intensity differences between the infrared absorptions of $^{13}CO_3^{2-}$ and $^{12}CO_3^{2-}$ in a 1:1 mixture. In this case, the sign of the coupling constant between adjacent molecules was negative, which meant that the lighter isotope would contribute more to the total infrared intensity (i.e., have a larger amplitude in that mode) than the heavier isotope. This is, in fact, exactly what he observed.

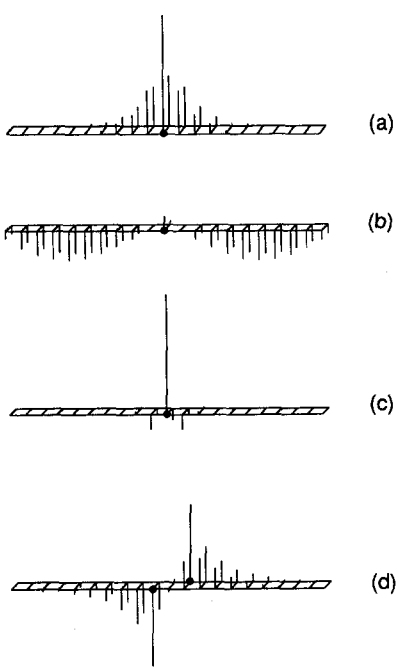

FIG. 7. Amplitudes of the O–O stretches for the model lattice of 40 molecules showing (a) and (b) two Raman active modes induced by the presence of a lighter isotope, ^{16}O ^{18}O, at the center of a heavier chain of $^{18}O_2$, (c) an infrared mode induced by $^{18}O_2$ in $^{16}O_2$, and (d) an infrared active mode due to the presence of two such impurities, i.e., a dimer site.

The frequencies for the pure and impurity doped solids are predicted to within 0.5% of their measured values (see Table I). Thus, this simple model accounts for the infrared fundamental, Raman fundamental, infrared combinations, and isotope-induced features. A simple linear chain of oxygens will not adequately explain these results due to the high symmetry of such a chain (i.e., the lack of cell doubling). Some kind of cell doubling must occur for any model to explain the presence of both Raman and infrared active modes. Moreover, the position of the low frequency combination band indicates that there is a rather large amount of dispersion along the chain, provided the assignment to a combination of zone boundary Raman and infrared modes is correct. In fact, the amount of dispersion along the appropriate k vector direction (i.e., along the chain) is on the order of the difference between the Raman and infrared zone center frequencies, which derive from the interaction force constant between the molecules of the primitive unit. It then follows that the interaction force constant f_2 between molecules of each pair is on the order of the interaction force constant f_3 between the pairs along the chain. We have assumed that they are in fact identical in our model. We have found that we still require one further interaction force constant between next-nearest neighbors. This is due to the fact that the zone-boundary Raman mode must occur at a substantially lower frequency than the zone center. Otherwise, we cannot explain the low frequency combination adequately. As long as the next-nearest-neighbor interaction force constant is substantial and positive, we find the proper behavior for the dispersion of both the infrared and the Raman branches as shown in Fig. 8.

We believe that the interaction that leads to this distortion of the oxygen lattice is linked to a spin-pairing transition that destroys the triplet nature of the isolated oxygen molecules as well as the antiferromagnetism that is characteristic of most phases of oxygen. Experimental difficulties prevent any type of magnetic measurement from being performed at the present time at these pressures. We are therefore unable to verify this prediction experimentally. An estimate of this pairing energy, however, follows from an average of the two spin-paired configurations $^1\Delta$ and $^1\Sigma$ since transitions of these two configurations from the $^3\Sigma$ ground state occurs simply as a result of pairing the spins of the triplet state

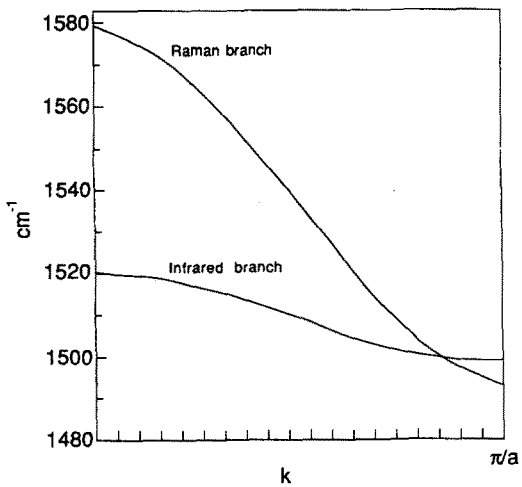

FIG. 8. Dispersion curves for the Raman and infrared branches that result from this model.

(ignoring any contribution from higher configurations). This pairing energy is an average of 1.63 and 0.98 eV or 1.3 eV. We note that our interpretation of this spin-pairing transition is consistent with the appearance of a band edge for this phase of oxygen at about 1.7 eV and is quite distinct from a previous explanation that presumed that the gap between the two configurations $\pi^4\pi^{*2}$ and $\pi^3\pi^{*3}$ was closing.[5] These bonding orbitals between adjacent oxygen molecules are nevertheless antibonding with respect to the oxygen molecular bonds. Therefore, we expect a weakening of the oxygen molecular bond, which is exactly what occurs. As pressure increases, the infrared band drops faster than the Raman band rises in frequency. This means that the force constant for the O–O bond is in fact decreasing over this pressure interval.

The appearance of two Raman bands in the sample with 6% ^{16}O ^{18}O in $^{18}O_2$ and their pressure dependences (Fig. 4) represents, as far as we have been able to determine, a unique example of the solid state effect of "mode pulling" due to an isotopic impurity in a molecular solid, although it may be more appropriate to term this effect impurity mode domination. We believe that the impurity has "pulled" two modes out of the vibron band by the nature of the extended interactions in this oxygen lattice. Due to the concentration of the ^{16}O ^{18}O isotope (6%) and the fact that even second nearest neighbors contribute to the interaction, these two modes become the bulk modes. What exactly are the natures of these two modes? In the simple model that we have constructed, two Raman active modes appear that consist of wholly symmetric bulk motions either in- or out-of-phase with the impurity [see Figs. 7(a) and 7(b)]. We believe that these two modes are responsible for the appearance of the two bands in the Raman of this sample and as the interaction force constants increase (and the diagonal force constant f_1 remains fixed), the higher frequency mode takes on more bulk character and less impurity character. It is as though the bulk and impurity modes are in resonance and increasing pressure tunes this resonance, which we know is not quite correct and that actually, due to long range interactions, the rather low concentration of the impurity (6%) is nevertheless sufficient to affect the entire solid. We note that this model also

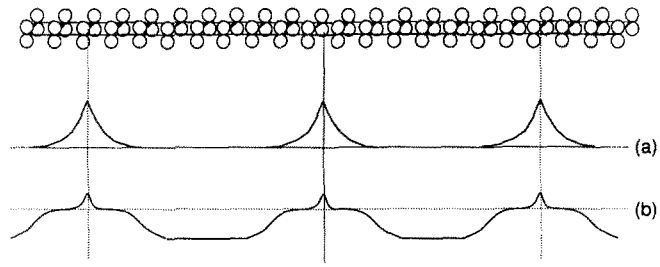

FIG. 9. Amplitude of the impurity induced modes for a "perfect" 6% distribution of impurity in an infinite chain model lattice. (a) Corresponds to Fig. 7(a) and (b) of this figure corresponds to Fig. 7(b).

explains the presence of an impurity infrared band whose frequency lies between the two Raman bands' frequencies and is due to sites of impurity pairs with the character shown in Fig. 7(d). This particular pair is simply representative of the character of each of a distribution of "pair sites", with different numbers of constituent $^{18}O_2$ molecules. We have not attempted to model this distribution or its effect on the intensity.

Now that we have developed a model and calibrated the force constants and interaction force constants, there remains the question of how appropriate the model is over greater pressure ranges as well as impurity concentrations. Unfortunately, quantitative application of our model over higher pressure or concentration is thus far limited by the model's inability to simulate the statistical distribution of impurities in an infinite lattice. In particular, the behavior of the Raman mode in Fig. 7(b) with increasing interaction force constant (due to increasing pressure) will depend critically on the actual distribution of the ^{16}O ^{18}O impurity in the lattice. A qualitative extension of our model, however, is possible and indeed appropriate. With an exactly 6% even distribution, for example, a ^{16}O ^{18}O would occur every 16.7 molecules or 8.3 primitive units along the chain of the model lattice. The Raman modes which are "pulled" out of such a vibron band are off the zone center, then, by $\pi/8.3a$ and have the amplitudes as shown in Fig. 9. This particular configuration is indeed the most probable one given the actual distribution of 6% ^{16}O ^{18}O in $^{18}O_2$, but there is a series of such configurations given by some random distribution function, and it is this distribution that must be modeled in order to properly represent the intensities and pressure and concentration dependences of the impurity-induced features. Qualitatively, the mode in Fig. 9(a) will spread and become delocalized as the interaction force constant increases (i.e., as pressure increases). Conversely, the mode in Fig. 9(b) will become more localized with increasing interaction force constant.

Thus, while we feel confident that our simple model quantitatively explains the appearances of the isotope-induced features, it is only able to qualitatively represent the pressure and concentrations dependence of these same features. We leave this most intriguing, but nevertheless complex problem to some future work.

CONCLUSION

We conclude that the ϵ phase of oxygen has a centric structure with two molecules per primitive unit, and that

there are very strong anisotropic intraplanar interactions that result in chains of oxygen pairs, where the interaction force constant between each molecule of the pair is the same as between pairs along the chain axis. The transition to ϵ-O_2 from the precursor δ-O_2 results from a zone boundary shear as well as a compression within the molecular oxygen planes, and a unique impurity mode domination occurs that can be pressure tuned when a ^{16}O ^{18}O molecule is present in an $^{18}O_2$ lattice. A model incorporating a linear chain of molecular oxygen pairs and three adjustable force constants has successfully explained the observed infrared and Raman features for a variety of isotopic mixtures.

ACKNOWLEDGMENTS

We thank Bob Mills and David Schiferl for their kind help in loading various cells and as well as their useful discussion. This work was supported by the Fundamental Research in Explosives (FRE) program at Los Alamos and was performed under the auspices of the US Department of Energy.

[1]C. A. English and J. A. Venables, Proc. R. Soc. London Ser. A **340**, 57 (1974).
[2]I. N. Krupskii, A. I. Prokhvatilov, Yu. A. Freiman, and A. I. Erenburg, Sov. J. Low Temp. Phys. **5**, 131 (1979).
[3]R. D. Etters, A. A. Helmy, and K. Kabushi, Phys. Rev. B **28**, 2166 (1983).
[4]D. Schiferl, D. T. Cromer, L. A. Schwalbe, and R. L. Mills, Acta Crystallogr. Sect. B **39**, 153 (1983).
[5]K. Syassen and M. Nicol, *Physics of Solids under High Pressure*, edited by J. S. Schilling and R. N. Shelton (North-Holland, New York, 1981), pp. 33–38
[6]B. I. Swanson, S. F. Agnew, L. H. Jones, R. L. Mills, and D. Schiferl, J. Phys. Chem. **87**, 2463 (1983).
[7]B. Olinger, R. L. Mills, and R. B. Roof, J. Chem. Phys. **81**, 5068 (1984).
[8]R. V. St. Louis and B. Crawford, J. Chem. Phys. **37**, 2156 (1962).
[9]B. R. Cairns and G. C. Pimentel, J. Chem. Phys. **43**, 3432 (1965).
[10]L. H. Jones, S. F. Agnew, B. I. Swanson, and S. A. Eckberg, J. Chem. Phys. **85**, 428 (1986).
[11]L. Merrill and W. A. Bassett, Rev. Sci. Instrum. **45**, 290 (1974).
[12]R. L. Mills, D. H. Liebenberg, J. C. Bronson, and J. C. Schmidt, Rev. Sci. Instrum. **51**, 891 (1980).
[13]G. J. Piermarini, S. Block, J. D. Barnett, and R. A. Forman, J. Appl. Phys. **46**, 2774 (1975).
[14]J. C. Decius, J. Chem. Phys. **23**, 1290 (1955).